ChemPlusChem

A Multidisciplinary Journal Centering on Chemistry

Chemistry Europe

European Chemical Societies Publishing

Accepted Article

Title: Enhanced Intracellular Accumulation and Cytotoxicity of Ferrocene-Ruthenium Arene Conjugates

Authors: Donát Gelle, Martin Lamač, Karel Mach, Ludmila Šimková, Róbert Gyepes, Lucia Sommerová, Andrea Martišová, Martin Bartošík, Tomáš Vaculovič, Viktor Kanický, Roman Hrstka, and Jiri Pinkas

To be cited as: *ChemPlusChem* 10.1002/cplu.202000022

Link to VoR: https://doi.org/10.1002/cplu.202000022

WILEY-VCH

Enhanced Intracellular Accumulation and Cytotoxicity of Ferrocene-Ruthenium Arene Conjugates

Donát Gelle,[a,b] Dr. Martin Lamač,[a] Dr. Karel Mach,[a] Dr. Ludmila Šimková,[a] Dr. Róbert Gyepes,[a,b] Lucia Sommerová,[c] Andrea Martišová,[c] Dr. Martin Bartošík,[c] Dr. Tomáš Vaculovič[d], Prof. Viktor Kanický[d] Dr. Roman Hrstka,[c,*] and Dr. Jiří Pinkas[a,*]

[a] J. Heyrovský Institute of Physical Chemistry, Academy of Sciences of the Czech Republic, v.v.i., Dolejškova 2155/3, 182 23 Prague 8, Czech Republic

[b] Department of Chemistry, Faculty of Education, J. Selye University, Bratislavská cesta 3322, 945 01 Komárno, Slovak Republic

[c] Regional Centre for Applied and Molecular Oncology, Masaryk Memorial Cancer Institute, Žlutý kopec 7, 65653 Brno, Czech Republic

[d] Department of Chemistry, Faculty of Science, Masaryk University, Kamenice 753/5, 62500 Brno, Czech Republic

* Correspondence to: Jiří Pinkas, tel. (+420) 266053735, e-mail: pinkas@jh-inst.cas.cz or Roman Hrstka, tel. (+420) 543133306, e-mail: hrstka@mou.cz.

Abstract

Coordination of arenophilic Cp*Ru$^+$ (Cp* = η^5-C_5Me_5) fragment to pendant aromatic ring(s) of either benzylferrocene (**1**) or dibenzylferrocene (**2**) gave air- and water- stable dinuclear (**4**) or trinuclear (**6**) ferrocene-ruthenium conjugates. Complexes were characterized by NMR, ESI-MS, cyclic voltammetry (CV), elemental analysis, and molecular structure of **4** was established by single crystal X-ray diffraction. Contrary to the starting ferrocenes **1** and **2**, conjugates **4** and **6** showed significant *in vitro* anticancer activity (up to IC_{50} 0.6±0.2 μM) against various cancer cell lines (A2780, SK-OV-3, MDA-MB-231). Differential pulse voltammetry (DPV) proved ca two times higher intracellular accumulation of **4** in comparison to **6** in all studied cell lines, which roughly corresponded to higher cytotoxicity of the former one.

Introduction

The success of cisplatin (*cis*-[$PtCl_2(NH_3)_2$]) in cancer therapy started an unflagging interest in development of new drugs based on transition metal complexes (so called metallodrugs). Among other metals, iron and ruthenium complexes play a prominent role. The first one thanks to the stability and versatility of ferrocene moiety led to the development of various cytostatic ferrocene derivatives.[1] The most studied ruthenium complexes are $(ImH)^+$[*trans*-$RuCl_4$(κ-*S*-dmso)(κ-*S*-Im)]$^-$ (NAMI A) and species of the RAPTA family of general formula [(η^6-arene)$RuCl_2$(pta)] (where pta = l,3,5-triaza-7-phosphatricyclo[3.3.1.1]dekane).[2] Both families of ruthenium species are characteristic for their low cytotoxicity and unprecedent anti-metastatic properties in animal model experiments. In addition, several other types of ruthenium coordination complexes such as $IndH^+$[*trans*-$RuCl_4$(κ-2-*N*-Ind)$_2$]$^-$ (where Ind = indazol) (KP1019) and Na^+[*trans*-$RuCl_4$(κ-2-*N*-Ind)$_2$]$^-$ (KP1339), (η^6-Biph)RuCl[(κ2-N,N-en)] (where Biph = biphenyl, en = 1,2−diaminoethane) (RAED), ruthenium cationic polypyridyl complexes and many others were intesively investigated as was recently reviewed.[3] However, there has been no approved metallodrug based on either iron or ruthenium in a clinical practice to date.

In order to increase the cytotoxic effect of the particular metallodrug, one can suggest an interconnection of the ferrocene derivative (generally used as a metalloligand) with a ruthenium complex into a single heterodinuclear complex. Indeed, in several cases a connection of the ruthenium and ferrocene part led to a substantial cytotoxicity boosting in comparison to separated parts.[4]

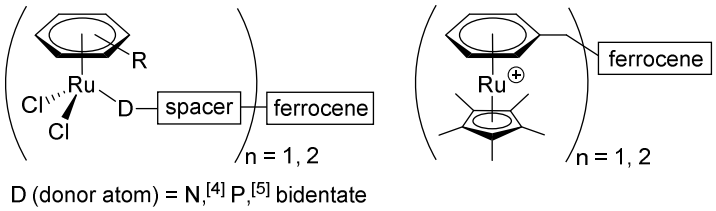

Chart 1 General formula of the most common cytotoxic ruthenium ferrocene conjugates (left) and conjugates studied in this work (right)

Most of dinuclear ruthenium-ferrocene conjugates (Chart 1, left side) were prepared by coordination of the ferrocene-tethered donor group to an easily accessible ruthenium dimer [(η^6-*p*-cymene)$RuCl_2$]$_2$. A variety of N-heterocycles (pyridines, imidazoles, piperidines) connected to ferrocene moieties *via* amido, ester or alkanediyl spacers were used as ligands for ruthenium coordination.[5] Formed conjugates were tested against ovarian (A2780,

A2780R) and colorectal (HT29) cancer cell lines, however, only modest activities were observed. A slightly higher cytotoxic efficiency (IC_{50} up to low μM) against A2780 and A2780R cell lines was found for ruthenium complexes with κ-*P*-coordinated diphenylphoshinoferrocene amido acids.[6] Smith and coworkers prepared 12 metallodendrimers, including some ferrocene-derived with [(η^6-*p*-cymene)Ru(X)] (X = Cl, pta) on their periphery. Among the metallodendrimer series, the ferrocene-derived ruthenium-pta dendrimers were found most active and induced more than 50% inhibition of A2780 and A2780R cell lines growth at 5 μM concentration of iron.[7]

Another family of conjugates are octahedral ruthenium complexes functionalized with ferrocene. A coordination of pyridine-tethered ferrocene to NAMI-A led to a conjugate with improved cytotoxicity, while the anti-metastatic activity typical for NAMI-A was preserved.[4b] In another example, a conjugate *fac*-[$RuCl_3$(NO)(dppf)] (where dppf = 1,1´-bis(diphenylphosphino)ferrocene) exerted ten times higher cytotoxicity against breast cancer cell line MDA-MB-231 in comparison to dppf.[4a] Ruthenium substituted vinylferrocene conjugates were prepared by hydroruthenation of ethynylferrocene with [RuClH(CO)(P-*i*Pr_3)].[8] The ruthenium-ferrocene and ruthenium-ferrocenium conjugates showed cytotoxicity against HT-29 (colon) and MCF-7 (breast) cancer cell lines in low micromolar region. The cationic conjugate possessed activity ca 2-3 times higher than the neutral one, which corresponded to its 2-4 times higher accumulation in cancer cells.[9] Very recently, a synthesis of dinuclear octahedral ruthenium complex with κ-*S*-coordinated ferrocenylthioether [Ru(tpy)Cl_2(mtpfc)] (where tpy=terpyridine, mtpfc = 3-(methylthio)-propyl}ferrocene) was published.[10] The complex showed a promising *in vivo* tumor growth inhibition along with increased survival rate of tumor bearing mice.

It should be noted, that there are also several examples of hetero di- and polynuclear ferrocene-spacer-(η^6-arene)ruthenium(cyclopentadienyl) complexes mentioned in the literature (i.e. complexes structurally closely related to the ones studied in this work).[11] However, these species were not evaluated for their biological properties.

Herein, we would like to present the preparation of new ferrocene-ruthenium cyclopentadienyl conjugates (Chart 1, right side) generated from either benzylferrocene or 1,1´-bisbenzylferrocene by coordination of pendant benzyl group(s) to one or two Cp*Ru (Cp* = η^5-C_5Me_5) fragment(s). Cytotoxicities of both complexes against human ovarian cancer cell lines (A2780, SK-OV-3) breast cancer cell line (MDA-MB-231) and human embryonic kidney cell line (HEK 293) were evaluated and correlated with uptake of compounds into the cells, their propensity to induce apoptosis and block cell migration.

Results and discussion

Ferrocenes synthesis

Benzylferrocene (**1)** was prepared as described previously from ferrocenebenzaldehyde by Et_3SiH reduction catalyzed by $TiCl_4$.[12] However, a prolonged time and increased amount of silane was needed to accomplish full conversion, whereas **1** was obtained in 17 and 34% yields in repeated experiments. 1,1´-Bisbenzylferrocene (**2**) was prepared by the reaction of respective $Li(C_5H_4Bn)$ with anhydrous $FeCl_2$ as we published previously.[13]

$[(\eta^5\text{-}C_5Me_4Bn)_2Fe]$ (**3**), a permethylated analogue of **2**, was prepared by an analogous procedure i.e. reaction of the corresponding lithium salt $Li(C_5Me_4Bn)$ with anhydrous $FeCl_2$. The formed ferrocene **3** was purified by crystallization. The species **3** is considerably more prone to oxidation than **2**, slowly oxidizing upon standing in air (even in the solid state). Ferrocene **3** was fully characterized by spectroscopic methods (NMR, ESI-MS), mp and elemental analysis (see experimental part).

Ruthenium-ferrocene conjugates synthesis

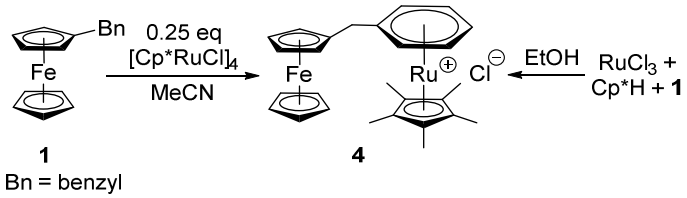

Scheme 1 Preparation of dinuclear ferrocene-ruthenium conjugate **4**

Preparations of targeted ruthenium-ferrocene conjugates were based on a strong arenophilicity of *in situ* generated species $[Cp^*Ru(MeCN)_3]Cl$ as previously described by Fairchild.[14] The reaction of $[Cp^*RuCl]_4$ with a slight excess of **1** (Scheme 1, left side) was performed in boiling acetonitrile for 18 h. The desired conjugate **4** was obtained in 53 % yield as a main product, while the excessive starting compound **1** could be easily removed by column chromatography. Finally, **4** was purified by crystallization, which led to a crystalline material suitable for X-ray crystallography. Alternatively, **4** could be prepared by the reaction of $RuCl_3$, Cp*H and **1** in refluxing ethanol (Scheme 1, right side) as was described previously for the preparation of $[Cp´Ru(\eta^6\text{-arene})]Cl$ (for $Cp´ = \eta^5\text{-}C_5H_5$)[15] (for Cp´ = Cp*)[16]. Initially, $RuCl_3$ was refluxed in ethanol and then an excess of Cp*H and **1** was added to the *in*

situ generated ruthenium(II) species . Refluxing of the mixture for 17 h gave, after workup, **4** in 60 % yield.

We also attempted to prepare [Cp*Ru(η^6-benzoylferrocene)]Cl by reaction of benzoylferrocene with $[Cp^*RuCl]_4$, however, results were ambiguous. While a NMR experiment in MeCN-d_6 indicated formation of desired [Cp*Ru(η^6-benzoylferrocene)]Cl in ca 10 mol% after 90 min of reaction, the preparative scale reaction gave very complex mixture of various products after 32 h (for details see SI). We propose that a decreased electron density of phenyl ring in benzoylferrocene led to its less stable η^6-coordination, which allowed a different reactivity of the Cp*Ru fragment.

While ligand **1** allowed coordination of only single ruthenium atom, ligand **2** could formally form both monoruthenated (**5**) and diruthenated (**6**) species. For synthetic reasons we further focused predominantly on preparation of **6**. The reaction (Scheme 2, left side) was performed in a similar manner as described above for **4**, with exception that an excess of $[Cp^*RuCl]_4$ was used. The reaction was followed by ^{1}H NMR spectroscopy (for details see experimental section), which indicated formation of **6** (80 mol %) and **5** (20 mol %) after 48 h. A further portion of $[Cp^*RuCl]_4$ into the mixture forced the reaction to completion and **6** was obtained in 92% after work-up.

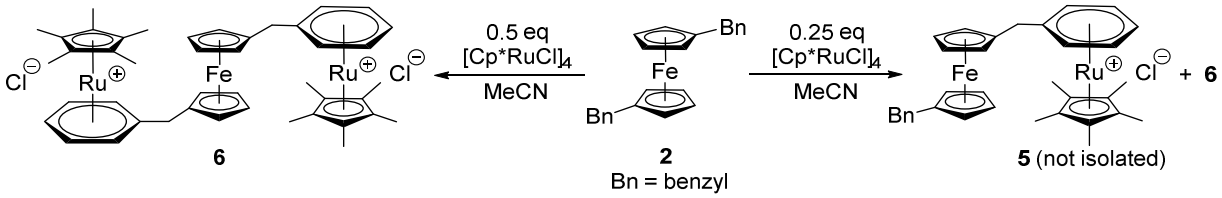

Scheme 2 Preparation of trinuclear ferrocene-ruthenium conjugate **6**

We also tried to prepare **5** by reaction of 0.25 equivalents of $[Cp^*RuCl]_4$ with excess of **2** (Scheme 2, right side, for details see SI) in refluxing MeCN. After the reaction proceeded, a mixture of **5** and **6** in ca 4/1 ratio was obtained. Unfortunately, we did not succeed in removing **6** (either by chromatography of crystallization) due to similar properties of both complexes.

In addition, we attempted to prepare a highly methyl substituted analogue of **6** by reaction of **3** with an excess of $[Cp^*RuCl]_4$ (for details see SI). Although the coordination of both benzyl groups was achieved (as proved by a characteristic downfield shift of aromatic protons about 1.2 ppm in ^{1}H NMR spectrum), we were not able to isolate the proposed product in a pure state, most probably due to a presence of paramagnetic oxidation products.

Complexes **4** and **6** are well soluble in chlorinated solvents, acetonitrile, methanol and sufficiently soluble in water. Their ^{1}H NMR spectra showed a characteristic down-field shift (ca 1.0 - 1.5 ppm) for the phenyl group coordinated to ruthenium atom in comparison to free phenyl group in **1** or **2**. Signal for C_5Me_5 groups had identical values in both ^{1}H and ^{13}C NMR spectra (δ_H/δ_C: 1.95/10.2 ppm).

Conjugates **4** and **6** are water stable compounds, both in the solid state and in solution. Their solutions in D_2O were measured by ^{1}H NMR spectroscopy after 1, 2, and 10 days (see Figure S8 in SI). Spectra showed a quantitatively non-changing pattern, however signals became broader and shifted with the solutions ageing. We propose that the dinuclear framework of the molecules remained unchanged, however, the ferrocene part slowly oxidized to a paramagnetic ferrocenium in air. It should be mentioned that both "isolated" parts of **4**, i.e **2** and [(η^6-toluene)RuCp*]Cl (**TolRuCl**) showed good stability in aqueous environment, although the former one is only sparingly soluble in water.

Molecular structure of 3 and 4

Ferrocene **3** crystallized in a triclinic space group *P*-$1\bar{}$ (No.2) with one molecule in the unit. Selected geometric parameters are given in SI (Table S1), molecular structure and selected bond distances and angles are given in Fig. 1. The molecule of **3** has a C_i symmetry with the point of inversion located on the central iron atom Fe1. The molecule showed an ideal staggered conformation of cyclopentadienyl rings with benzyl substituents oriented antiperiplanarly. Phenyl rings are oriented away from the ferrocene core and they are almost perpendicular (88.59 °) in respect to cyclopentadienyl rings. Molecules of **3** are connected within a crystal structure *via* a π-π stacking of phenyl (with interplane distance 3.172 Å) and Cp* rings (with interplane distance 3.641 Å), which creates aromatic and ferrocene domains (see Figure S9 in SI).

10.1002/cplu.202000022

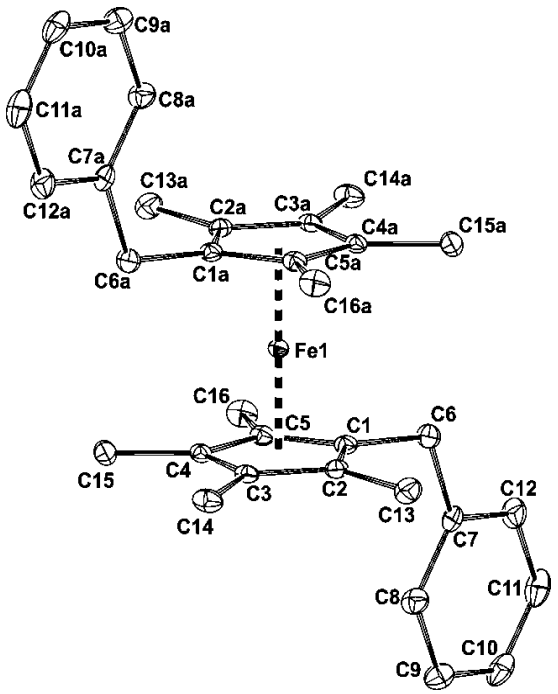

Figure 1 Molecular structure of **3** at the 30% probability level with atom labeling. Hydrogen atoms are omitted for clarity. Selected bond distances (Å) and angles (°): Fe-$Cg_{(C1-C5)}$ 1.6500(7), C-$C_{(ring\ C1-C5)}$ 1.426(2) − 1.433(2), C-$C_{(ring\ C7-C12)}$ 1.378(3) − 1.394(3), C1-C6-C7 114.10(13).

Dinuclear complex **4** crystallized in a monoclinic space group *C*2/*c* (No.15) with 8 molecules in the unit. Selected geometric parameters are given in SI (Table S1), molecular structure and selected bond distances and angles are given in Fig. 2. Environments of both metals possessed a metallocene arrangement with almost coplanar rings (angle 2.90 ° for Cp*-arene, 3.73 ° for ferrocene unit). Both metals adopt the same position (syn) in respect to bridging $C_6H_5CH_2C_5H_4$ ligand, while the intermetal distance is 6.555 Å. Similarly to **3**, phenyl group in **4** is oriented away from the ferrocene core, while the angle between phenyl (C11-C16) and cyclopentadienyl (C18-C22) plane is 104.93 °. Ferrocene rings are almost in ideal eclipsed conformation (torsion angle C18-$Cg_{(C18-C22)}$-$Cg_{(C23-C27)}$-C23 is 0.19 °). Molecule packing in crystal (Figure S10 in SI) showed, besides phenyl rings π-π stacking (a distance between planes is 3.118 Å), π-π stacking between Cp* rings (interplane distance 3.622 Å), which led to a zig-zag connection of molecules.

10.1002/cplu.202000022

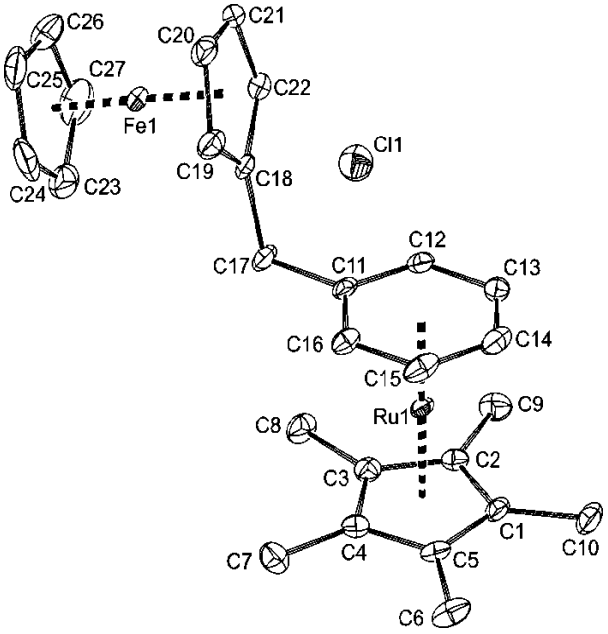

Figure 2 Molecular structure of **4** at the 40% probability level with atom labeling. Hydrogen atoms are omitted for clarity. Selected bond distances (Å) and angles (°): Ru1-$Cg_{(C1-C5)}$ 1.8014(14), Ru1-$Cg_{(C11-C16)}$ 1.7021(13), Fe1-$Cg_{(C18-C22)}$ 1.6377(15), Fe1-$Cg_{(C23-C27)}$ 1.6443(19), $Cg_{(C1-C5)}$-Ru1-$Cg_{(C11-C16)}$ 178.29(6), $Cg_{(C18-C22)}$-Fe1-$Cg_{(C23-C27)}$ 177.11(9), C11-C17-C18 108.3(2).

Electrochemistry

Electrochemical behavior of ferrocenes **1**-**3**, ruthenium-ferrocene conjugates **4** and **6** and **TolRuCl** was studied by cyclic voltammetry in non-aqueous MeCN solutions (for details see Experimental part). Results are summarized in Table 1 and cyclic voltammograms of **1**, **4**, and **TolRuCl** are depicted in Fig. 3.

All three ferrocene complexes **1**-**3** displayed a reversible oxidation wave characteristic for Fe^{3+}/Fe^{2+} couple of ferrocene core. Benzyl group(s) behaved as rather electroneutral one as could be seen from electrochemical Fe^{3+}/Fe^{2+} potentials in **1** (0.01 V) and **2** (−0.04 V), with values close to ferrocene. As expected, the presence of eight electron donating methyl groups in **3** led to its easier oxidation (shift by 370 mV to more negative values) in comparison to **2**. It should be noted that electrochemical reduction of **1**-**3** did not proceed up to a potential of −3.28 V.

On the other hand, reduction of cationic ruthenium complexes **4**, **6**, and **TolRuCl** proceeded in a diffusion controlled irreversible wave (see Fig. S5-S7 in SI) within a narrow region from −2.66 V to −2.58 V, while two nearby reduction steps (at −2.63 and −2.58 V)

were observed for **6**. The process is consistent with one-electron reduction of stable 18-electron cationic complexes to reactive neutral 19-electron ones. The reactive 19-e species is supposed to undergo stabilization by either dimerization or hydrogen atom abstraction from a solvent as was previously published for cationic [(η^6-arene)RuCp*] complexes.[17] Electrochemical potentials for Fe^{3+}/Fe^{2+} couple were shifted in conjugates **4** and **6** to more positive values (ca 70 mV per one Cp^*Ru^+) in respect to "free" ferrocenes **1** and **2**, which reflected the presence of one or two electropositive Cp^*Ru^+ fragments in conjugates. Similar positive shift in E°(Fe^{3+}/Fe^{2+}) was observed in [ferrocene-spacer-(η^6-C_6H_5)RuCp*] (150 mV for spacer = CH_2CH_2; 170 mV for spacer = CH=CH, and 155 mV for spacer = C≡C) conjugates.[11a] Furthermore, cationic complexes **4**, **6**, and **TolRuCl** showed an extra irreversible oxidation wave in 0.65-0.72 V region. We tentatively assigned this process to Ru^{3+}/Ru^{2+} couple as the wave is missing in free ferrocenes **1-3** voltammograms.

Table 1 Cathodic peak potentials (E_{pc}), anodic peak potentials (E_{pa}) and standard redox potentials (E^0) of ferrocenes **1-3**, ruthenium-ferrocene conjugates **4** and **6**, and **TolRuCl**.[a]

	E_{pc} [V]	**E^0 [V]**	**E_{pa} [V]**		
		Fe^{3+}/Fe^{2+}	Ru^{3+}/Ru^{2+}		
1	-	0.01	-	-	1.57
2	-	−0.04	-	-	1.42
3	-	−0.41	-	1.12	1.48
4	−2.62	0.08	0.72	-	1.58
6	−2.63, −2.58	0.10	0.65	-	n.a.
TolRu 1	−2.66	-	0.69	-	1.55

[a] Conditions: measured in Acetonitrile using 0.1 M Bu_4NPF_6 as an electrolyte; glassy carbon electrode. The potentials are referenced to ferrocenium/ferrocene couple. n.a. character of oxidation peak did not allow correct E_{pa} determination

10.1002/cplu.202000022

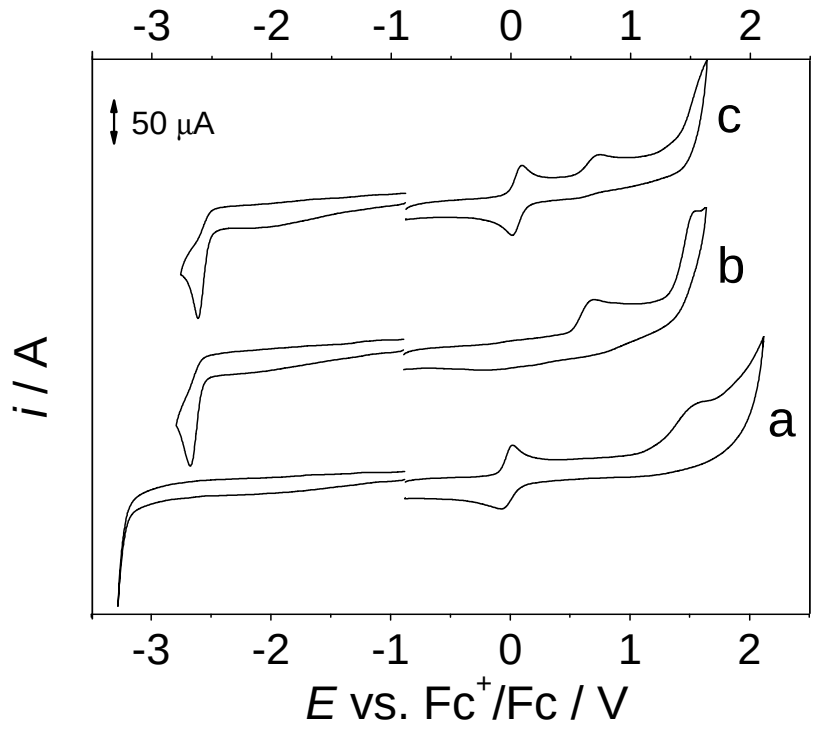

Figure 3 Cyclic voltammograms of **1** (a), **4** (c), and **TolRuCl** (b). (1 mM solutions in MeCN, scan rate 100 mV).

Determination of cell uptake by DPV

An initial prerequisite for efficient performance of any active pharmaceutical ingredient (API) is its internalization into cells. The redox active ferrocene core, involved in all prepared species, is ideally suited as an electrochemical probe for determination of the particular species uptake into cells. We have shown earlier that an electrochemical technique called differential pulse voltammetry (DPV) offers a simple and quick approach to quantitatively determine ferrocene derivatives in low μM range not only in solution, but also inside cancer cells.[18] This was possible due to a reversible one-electron oxidation of the iron atom, which resulted in an oxidation peak with E_P close to +150 mV and which height reflected concentration of the ferrocene. In this work, all tested compounds were first diluted in culture media to a final concentration of 2 μM, and subjected to DPV to determine their oxidation peaks. Interestingly, under the conditions optimized in our previous reports,[18] only ferrocene-ruthenium conjugates **4** and **6** yielded well-developed oxidation peaks (Figure S14). Potential explanation may be that the ionic fragment obviously supported solubilization of **4**

and **6** in biological aqueous environment (as both complexes were easily soluble in D_2O as was shown above), however, its proper role in transport is to be elucidated. Ferrocene compounds **1-3,** on the other hand, are uncharged and highly hydrophobic, thus less soluble in aqueous solutions, making their determination at lower concentrations more difficult (only negligible iron oxidation signals were recorded at this concentration). Indeed, when we increased concentrations to 25 µM, ferrocene compounds **1** and **2** produced iron oxidation signals, while **TolRuCl** and [η^6-toluene)RuCp*]PF_6 (**TolRuPF**) gave no responses even at 100 µM due to the lack of iron atom (Figure S14 Inset).

We also checked the stability of the two active compounds **4** and **6** in time, and found out that no significant degradation of either of them occurred over 12 days during which they were stored at 37°C in culture media (Figure S15). This finding is especially important when analyzing penetration of **4** and **6** into cancer cells (see below), since the cells were cultured in media with both compounds for 16 h, suggesting that no apparent degradation of the compounds occurred over this time period.

Based on above studies performed in solution, we then applied DPV technique to measure an uptake of **4** and **6** into three different cancer cell lines (A2780, SK-OV-3, MDA-MB-231) and into embryonic HEK-293 cells (Figure 4A). As expected, the control sample, i.e. cells without **4** or **6**, did not yield any signal. However, specific signals were observed for both **4** and **6** indicating that these compounds penetrated into all studied cell lines. Interestingly, compound **4** yielded higher signals as compared to **6** when analyzing selected cell lines. To support the findings obtained with DPV, which measures an iron signal, we used also ICP-MS, an analytical technique convenient for elemental determinations, to quantify the absolute amount of Ru (Figure 4B). ICP-MS measurements confirmed results from DPV, although seemingly the amounts of **4** and **6** look similar. It should be, however, noted that **4** contains only single ruthenium atom compared to **6** bearing two ruthenium atoms, which translates into a double amount of **4** over **6**, confirming DPV data. We suppose that significantly higher accumulation of **4** in cells may be due to its lower overall size and/or its higher lipophilicity in comparison to **6**. This was demonstrated by a Shake flask method, where we experimentally determined LogP values to be −0.383 for **4** and −0.847 for **6**, respectively, where only the former value falls into "druggable region" (logP in region from −0.4 to 5.6).[19] The positive effect of metallodrug lipophilicity on their cellular uptake was recently mentioned by Kostrhunova et al.[20]

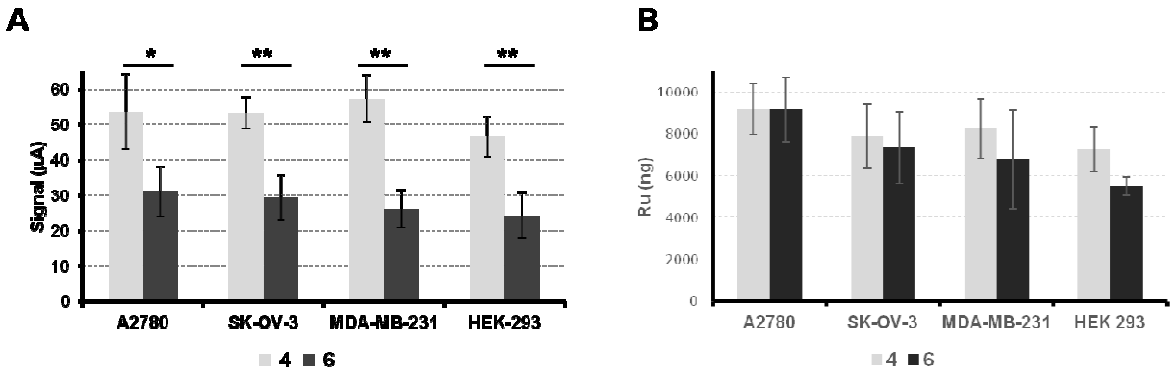

Figure 4 Cellular uptake of 2 µM **4** and **6** into various cell lines after 16 h incubation, as measured by (A) DPV, where signal was a current from iron oxidation and (B) ICP-MS that quantified absolute amount of ruthenium (Ru), where specific yields of Ru were calculated per gram of freshly collected cell mass. The results are an average of 4 technical replicates from 2 independent experiments, plotted as a mean ± SD where * is (P≤0.05), ** (P≤0.01).

Determination of antitumor effects

Cytotoxicities of **1**-**6**, **TOLRuCl**, **TOLRuPF** and cisplatin (serving as a positive control) against cancer cell lines A2780, SK-OV-3, MDA-MB-231 and embryonic HEK-293 cells were evaluated by MTT assay (Table 2). Briefly, ferrocenes were found mostly inactive, while ruthenium-ferrocene conjugates showed high antitumor activity against all cancer cell lines. Likewise, **4** possessed up to one order higher efficacy in comparison to **6**, which corresponds to its higher internalization into cells as shown in Figure 4.

It should be noted that both **TolRu** compounds showed activities slightly lower in comparison to values published previously by Loughrey et al. (e.g. IC_{50} for **TOLRuPF** against MDA-MB-231 cell line were found to be 20.8 µM).[16b, 21]

The comparison of cytotoxic activity of equimolar amounts of mono-nuclear complexes **1** and TolRuCl with **4** and in a 1: 2 ratio (Table 2) with **6** highlighted the importance of the connection between the ruthenium and ferrocene part, which was associated with clearly increased cytotoxicity in comparison with the separated parts.

Table 2 Cytotoxicities (IC_{50}, [µM]) of tested compounds against cell lines as listed after 72 h treatment.

	A2780	SK-OV-3	MDA-MB-231	HEK-293
1	47.7±3.4	>100	>100	>100

2	>100	>100	>100	>100
3	71.2±14.6	>100	>100	>100
4	0.6±0.2	24.8±3.7	12.0±2.5	1.0±0.2
6	6.6±0.8	55.7±11.3	30.8±3.9	12.7±0.3
TolRuCl	40.1±12.4	>100	42.3±3.4	43.4±11.6
TolRuPF	30.1±11.6	>100	72.6±12.8	56.3±11.8
1+TolRuCl (1:1)	35.6±3.3	91.5±22.4	53.0±1.0	33.7±7.9
1+TolRuCl (1:2)	52.4±6.2	>100	71.5±6.4	56.6±1.2
cisplatin	1.7±0.3	5.6±1.0	3.7±0.6	3.8±0.5

Compounds **4** and **6** were thus subjected for subsequent analysis of cell death mechanism associated with cytotoxic effects of these compounds. The induction of apoptosis was investigated using Annexin V/PI staining, which enables detection of both early and late apoptotic cells (Figure 5). Both compounds (**4** and **6**) induced apoptosis in breast cancer cells MDA-MB-231with similar intensity. On the other hand, in remaining cell lines **4** induced apoptosis with greater efficiency compared to **6**, which is in agreement with ability of **4** to penetrate into cells as well as with results from MTT assay.

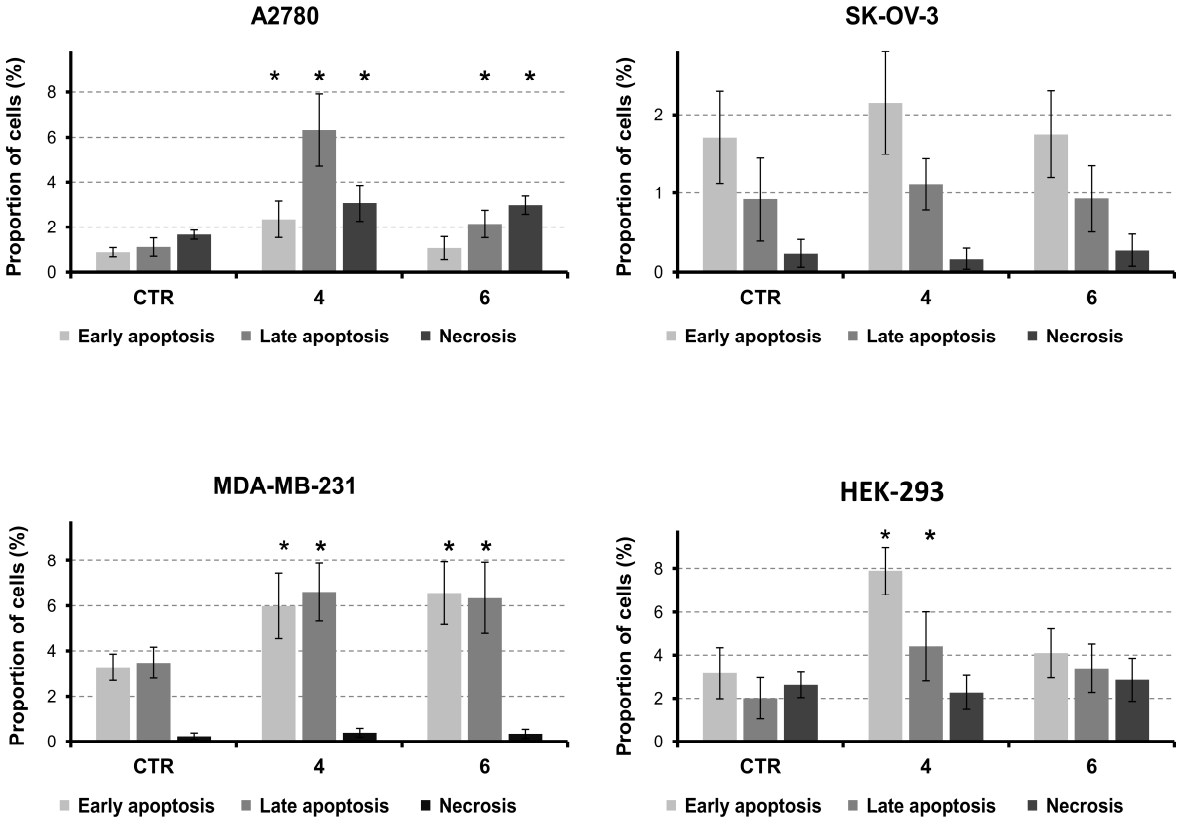

Figure 5 The induction of apoptosis was analyzed by Annexin V-FITC/PI FACS double staining assay for indicated cell lines. *apoptotic cells exposed to **4** and/or **6** as indicated showing significant changes (P<0.05) in comparison with untreated (CTR) cells.

Flow cytometry analysis of cell cycle perturbations was performed in all tested cell lines exposed to 10 μM concentrations of **4** or **6** at 48 hrs of compound exposure. The results of the cell cycle distribution consisting of averages of at least 3 independent experiments are shown in Figure 6. Interestingly, in all cancer cell lines we observed clear induction of G1 cell cycle arrest predominantly in response to treatment with **4**, albeit with marginal significance (P=0.08) in SK-OV-3 cells. In contrast, the treatment with **4** led to the accumulation of HEK-293 cells in G2/M phase of cell cycle. Cell cycle changes in cells exposed to **6** were less dramatic compared to **4**, while only A2780 showed significant accumulation of cells in G1 phase of cell cycle. This data indicates that these compounds influence cell cycle by different mechanism in comparison with cisplatin characterized by induction of cell cycle arrest in S and/or G2/M phase.[22]

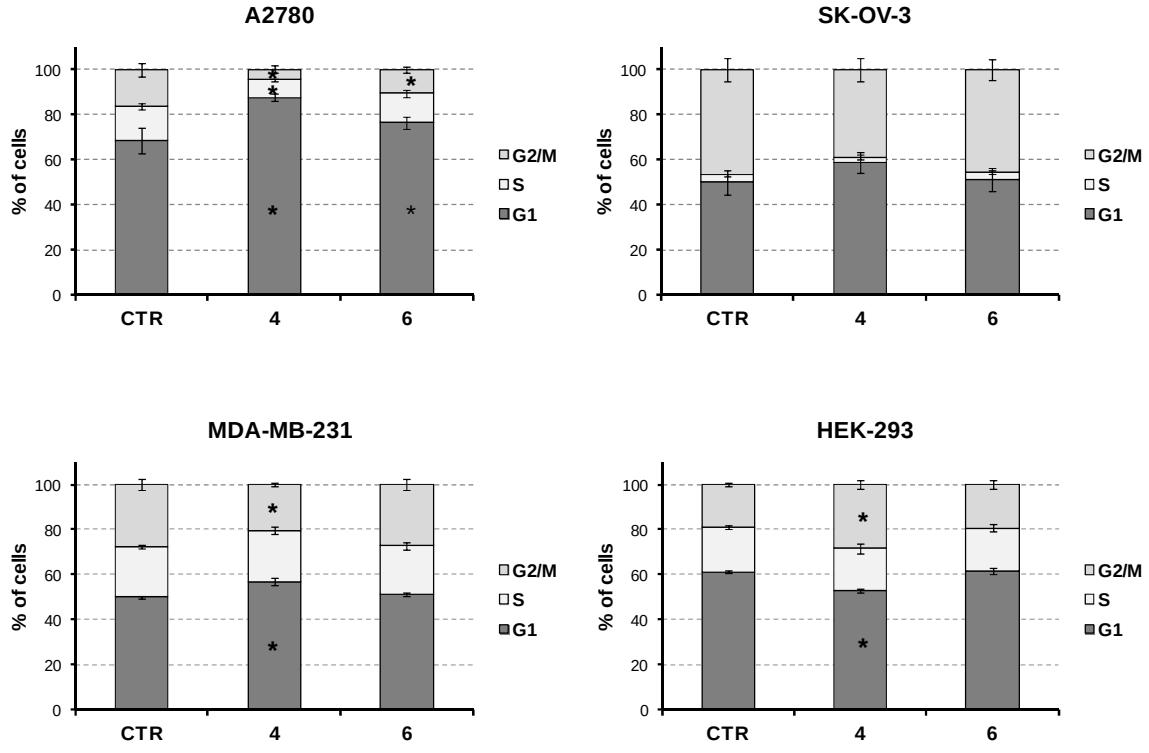

Figure 6 Cell cycle perturbations of selected cell lines exposed to **4** or **6**. *significant changes (P<0.05) in proportion of cells accumulated in particular phases of cell cycle.

To study potential migrastatic activity of **4** and **6**, we used wound healing assay. In cisplatin resistant SK-OV-3 cells we observed almost similar suppressive effect of **4** and **6**, while both **TolRuCl** and **TolRuPF** showed only limited migrastatic activity even at 100 μM concentration (Figures 7, S16 and S17). In parallel the cytotoxicity of above mentioned compounds was tested also for 24 h. MTT assay in SK-OV-3 cells revealed only low cytotoxicity in response to **4** (Table 3), thus supporting that **4** and **6** exhibit similar anti-migration effects towards SK-OV-3 cells. Conversely in MDA-MB-231 cells, **4** showed significantly greater migrastatic effectiveness against these highly metastatic breast cancer cells compared to **6** showing similar anti-migratory activity as **TolRu** complexes (Figures 7, S18 and S19). However, it should be considered that the high cytotoxicity of **4** against MDA-MB-231 cells (Table 3) may significantly distort the results of the migration assay.

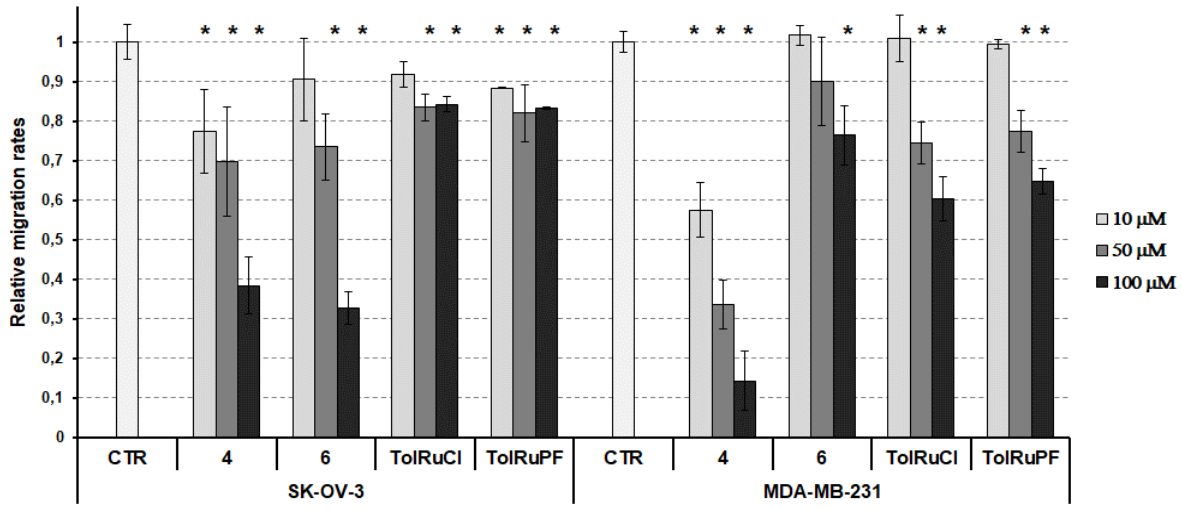

Figure 7 Wound healing assay for SK-OV-3 and MDA-MB-231 cells exposed to compounds as indicated: **4**, **6**, **TolRuCl** and **TolRuPF**. *P<0.05 compared to CTR.

Table 3 Cytotoxicities (IC_{50}, [μM]) of tested compounds against cell lines as listed after 24 h treatment.

	A2780	SK-OV-3	MDA-MB-231	HEK-293
4	9.1±3.1	136.7±46.6	38.5±10.2	3.5±0.2
6	89.3±12.5	>200	>200	150.8±4.0
TolRuCl	>200	>200	>200	141.1±11.0
TolRuPF	>200	>200	>200	139.3±15.5

Conclusions

We have shown that incorporation of arenophilic Cp*Ru$^+$ fragment into 1-benzylferrocene (**1**) and 1,1´-dibenzylferrocene (**2**) proceeded smoothly and resulted in corresponding air- and water- stable dinuclear (**4**) and trinuclear (**6**) ferrocene-ruthenium conjugates. The conjugation of lipophilic ferrocenes to ionic ruthenium fragment dramatically improved biological performance of conjugates against cancer cell lines. We have found (using electrochemical methods) increased intracellular accumulation of conjugates in comparison to starting ferrocenes following the order **1** ≈ **2** << **6** < **4**. The order further correlated with the increased species cytotoxicities against cancer cell lines, where the most active **4** overperformed cisplatin in A2780 cell line. Cell cycle analysis showed that treatment of cancer cell lines with **4** led to an induction of G1 block, which anticipated a mechanism different to that known for cisplatin. In addition, **4** exhibited significant migrastatic properties at concentrations below IC_{50}.

In conclusion, the work provided new examples of conjugated APIs, which display higher efficacy than simple summation of their isolated parts. It seems that investigations of similar types of API conjugates have become a current trend of metallodrugs research as was recently reviewed.[23]

Experimental part

Manipulation of air sensitive compounds was carried out under an argon atmosphere using standard Schlenk techniques. Anhydrous acetonitrile was obtained from Sigma Aldrich and stored over MS 3Å. Ethanol was used after stripping with argon for 40 min. $[Cp^*RuCl]_4$ was either obtained from commercial vendor (Strem Chemicals) or prepared by literature procedure.[24] Following materials **1**,[12] **2**,[13], **TolRuCl**[14], and **TolRuPF**,[21] were prepared by published procedures. Benzoylferrocene, $TiCl_4$, Cp*H, and Et_3SiH were obtained from Sigma Aldrich. Anhydrous $RuCl_3$ was obtained from Strem Chemicals.

NMR spectra were recorded on a Varian Mercury 300 (^{1}H at 300 MHz and ^{13}C at 75 MHz) spectrometer at 25°C. Chemical shifts are given relative to solvent signals (dmso-d_6, δ_H/δ_C 2.50/39.52 ppm; $CDCl_3$, δ_H/δ_C 7.26/77.16 ppm). High-resolution mass spectrometry (HRMS) spectra were measured with a Bruker MicrOTOF-QIII spectrometer on acetonitrile solutions of the samples. Electrospray ionization source in a positive mode was used for all

analyses and a calibration on sodium formate clusters was performed. Melting points were determined on a Koffler block and were not corrected. Elemental analyses were carried out on a FLASH EA1112 CHN-O Automatic Elemental Analyzer (Thermo Scientific).

The electrochemical behaviour of all samples was studied by cyclic voltammetry (CV) using a glassy carbon stationary electrode (area ca. 1 mm^2). The CV measurements were also performed at hanging mercury drop electrode (HMDE), however the oxidation of chloride anions at mercury electrode (at −0.58 V *vs.* Fc^+/Fc) preclude correct measurements in region from ca −0.5 V to −0.7 V. Solutions of the samples in MeCN (LC-MS Chromasolv®, ≥99.9 %, Fluka) at concentration 0.1, 0.5, and 1.mM were used for the measurement. The 0.1 M solution of terabutylammonium hexafluorophosphate (Bu_4NPF_6) of purissimum quality (TCI, >98.0 %) serving as the supporting electrolyte, was deoxygenated by argon. Ferrocene (Fc) purchased from Sigma-Aldrich was used as inner standard. For all electrochemical experiments a standard three-electrode system was applied. The auxiliary electrode was made of a platinum wire or platinum foil and a saturated calomel electrode (SCE) separated from MeCN solution by a salt bridge served as the reference electrode. All analytical experiments were carried out in an undivided 10 ml cell. All electrochemical experiments were conducted by the analog potentiostat PA4 with an XY recorder, both Laboratorní přístroje Praha. The redox potentials were stated against the ferrocenium/ferrocene couple (Fc^+/Fc).

Diffraction data for **3** and **4** were collected on a Nonius Kappa diffractometer equipped with a Bruker APEX II detector (MoK_α radiation, λ = 0.71073 Å) and were processed by the diffractometer software. The phase problem was solved by intrinsic phasing and the obtained structure models were refined by full matrix least squares on F^2 using the SHELX program suite.[25] All non-hydrogen atoms were refined anisotropically. Hydrogen atoms were placed into idealized positions and refined isotropically using the riding model. Molecular graphics was generated by using the PLATON program.[26]

CCDC numbers 1958339 and 1958338 contain supplementary crystallographic data deposited for **3** and **4**, respectively. These data can be obtained free of charge from The Cambridge Crystallographic Data Centre via www.ccdc.cam.ac.uk/data_request/cif.

Preparation of **3**

To a stirred yellow solution of 5-benzyl-1,2,3,4-tetramethylcyclopentadiene (a mixture of isomers, 1.50 g, 7.08 mmol) in THF (60 ml) was slowly dropped a solution of *n*-butylllithium in hexane (4.50 ml, 1.6M, 7.20 mmol), which caused a mixture color change to orange. The mixture was stirred for 2 h, solid $FeCl_2$ (0.44 g, 3.5 mmol) was added and the

mixture was refluxed for further 16h. The mixture was cooled to room temperature and volatiles were removed in vacuum. A solid residue was purified by chromatography on silica with cyclohexane as an eluent. The product was obtained as a yellow-orange oil, which spontaneously solidified upon storing overnight at room temperature. The product was washed with methanol (3 × 2 ml) and dried in vacuum. Yield 1.21 g (72%). Crystals suitable for X-ray analysis were obtained by recrystallization of **3** from boiling MeOH under argon. R_f = 0.5 cyclohexane. M.p. 127 °C. ^{1}H NMR ($CDCl_3$): 1.74 (s, 24H, C_5Me_4); 3.58 (s, 4H, CH_2Ph); 7.05 - 7.15 (m, 6H, CH_2Ph); 7.19 - 7.25 (m, 4H, CH_2Ph). $^{13}C\{^1H\}$ NMR ($CDCl_3$): 9.8, 10.0 (C_5Me_4); 31.5 (CH_2); 78.9, 79.5 (C_5Me_4, CMe); 81.7 (C_5Me_4, C_{ipso}); 125.6, 128.2, 128.3 (*Ph*, *C*H); 142.0 (*Ph*, C_{ipso}). ESI-HRMS, *m*/*z*: calcd. for $C_{32}H_{38}Fe$ $[M]^+$: 478.2323, found 478.2316. Elemental analysis calculated for $C_{32}H_{38}Fe$ (478.47): C, 80.32; H, 8.01; found: C, 80.44; H, 7.85%.

Preparation of **4**

a) using $[Cp^*RuCl]_4$ as a precursor

To a solid mixture of **1** (163 mg, 0.59 mmol) and $[Cp^*RuCl]_4$ (160 mg, 0.14 mmol) was added MeCN (10 ml) and the resulting suspension was refluxed for 18h. The resulting brown mixture was purified by column chromatography on alumina. First elution with CH2Cl2 gave trace amount of starting **1**. The second elution with a mixture CH_2Cl_2/MeOH (1/1, v/v) gave **4** as an orange-brown glassy solid. The product was further purified by crystallization (diffusion of Et_2O into CH_2Cl_2 solution of **4**. The obtained brownish crystals were suitable for X-ray analysis. Yield 172 mg (53 %).

b) using $RuCl_3$ as a precursor

To an anhydrous $RuCl_3$ (79 mg, 0.38 mmol) was added ethanol (10 ml) and the mixture was refluxed for 1h (color changed from dark brown to dark green). The mixture was cooled to room temperature, Cp*H (103 mg, 0.76 mmol), **1** (210 mg, 0.76 mmol) was added and the mixture was refluxed for 17h. After cooling to room temperature, volatiles were removed in vacuum. The solid residue was purified by column chromatography on alumina. Initial elution of the column with CH_2Cl_2 gave unreacted **1** (140 mg). Subsequent elution with a mixture CH_2Cl_2/MeOH (1/1, v/v) gave **4** as a yellow solid. Yield 125 mg (60 % in respect to $RuCl_3$). M.p. 205 °C (decomp.) ^{1}H NMR (dmso-d_6): 1.95 (s, 15H, C_5Me_5); 3.29 (s, 2H, CH_2); 4.11 (pseudo t, J_{HH} = 1.7 Hz, 2H, C_5H_4); 4.13 (s, 5H, C_5H_5); 4.15 (pseudo t, J_{HH} = 1.7 Hz, 2H, C_5H_4); 5.85-5.96 (m, 5H, *Ph*). ^{1}H NMR (D_2O): 1.96 (s, 15H, C_5Me_5); 3.34 (br s, $\nu_{½}$ = 4.2 Hz, 2H, CH_2); 4.24 (br s, $\nu_{½}$ = 8.1 Hz, 9H, C_5H_5 and C_5H_4); 5.70-5.81 (m, 5H, *Ph*). $^{13}C\{^1H\}$ NMR

(dmso-d_6): 10.2 (C_5Me_5); 32.0 (CH_2); 67.6, 67.7 (C_5H_4, *C*H); 68.5 (C_5H_5); 86.6 (C_5H_4, C_{ipso}); 86.7, 87.3, 87.4 (*Ph*, *C*H); 95.5 (C_5Me_5); 102.5 (*Ph*, C_{ipso}). ESI-HRMS, *m*/*z*: calcd. for $C_{27}H_{31}FeRu$ $[M–Cl]^+$: 513.0828, found 513.0824. Elemental analysis calculated for $C_{27}H_{31}ClFeRu \cdot 0.25\ Et_2O$: C, 59.37; H, 5.96; found: C, 59.93; H, 5.83%.

Preparation of **6**

A suspension of $[Cp^*RuCl]_4$ (451 mg, 0.41 mmol) in MeCN (10 ml) was heated to 90 °C until a complete dissolution of the solid phase did not occurred (ca 40 min). The formed orange solution was transferred into a suspension of **2** (300 mg, 0.82 mmol) in MeCN (10 ml) and the reaction mixture was refluxed for 48h. The ^{1}H NMR analysis of the mixture showed a formation of **6** (ca 80 mol%), besides monoruthenated species **5** (ca 20 mol %). To accomplish the reaction, an extra portion of $[Cp^*RuCl]_4$ (123 mg, 0.11 mmol) was added into the mixture and the mixture was refluxed for additional 12 h (after that **5** was not detected by ^{1}H NMR). Volatiles were removed in vacuum and the crude product was purified by chromatography on alumina with a MeOH/CH_2Cl_2 (12/1, v/v) mixture as an eluent. A brown band was collected and gave after solvent evaporation a brown waxy solid. The solid was further purified by crystallization from CH_2Cl_2/Et_2O mixture to give pure **6** as a yellow microcrystalline solid. Yield 687 mg (92 %).

M.p. 250 °C (decomp.) ^{1}H NMR (dmso-d_6): 1.95 (s, 30H, C_5Me_5); 3.26 (s, 4H, CH_2); 4.06, 4.10 (2 × pseudo t, 2 × J_{HH} = 1.7 Hz, 2 × 4H, C_5H_4); 5.87-5.99 (m, 10H, *Ph*). ^{1}H NMR (D_2O): 1.94 (s, 30H, C_5Me_5); 3.08 (br s, $\nu_{½}$ = 31 Hz, 4H, CH_2); 4.40 (br s, $\nu_{½}$ = 60 Hz, 8H, C_5H_4); 5.63-5.80 (m, 10H, *Ph*). ^{13}C{^{1}H} NMR (dmso-d_6): 10.2 (C_5Me_5); 31.7 (CH_2); 68.4, 68.6 (C_5H_4, *C*H); 86.7 (*Ph*, *C*H); 86.9 (C_5H_4, C_{ipso}); 87.3, 87.4 (*Ph*, *C*H); 95.5 (C_5Me_5); 102.5 (*Ph*, C_{ipso}). ESI-HRMS, *m*/*z*: calcd. for $C_{44}H_{52}ClFeRu_2$ $[M–Cl]^+$: 875.1214, found 875.1225; calcd. for $C_{44}H_{52}FeRu_2$ $[M–2Cl]^{2+}$: 420.0766, found 420.0764. Elemental analysis calculated for $C_{44}H_{52}Cl_2FeRu_2 \cdot 0.5\ Et_2O$: C, 58.35; H, 6.07; found: C, 59.12; H, 5.94%.

Biological experiments

Differential pulse voltammetry (DPV)

DPV experiments were performed at a scan rate of 10 mV/s and step potential of 5 mV, using µSTAT8000 multipotentiostat (DropSens, Llanera, Spain) at a screen-printed electrochemical array formed by eight 3-electrode electrochemical cells with carbon-based working electrodes (DRP-8X110 from DropSens, Llanera, Spain). During stability experiments, we prepared 2 µM solutions of **4** and **6** and incubated them in culture media (without cells) for desired time

at 37°C and then measured by DPV by casting 50 µl of the solution at the electrode surface. During cellular uptake experiments, cell pellets were first resuspended in 100 µl of 100 mM sodium phosphate buffer, pH 6.0 and the suspension was ultrasonicated for 1 min to lyse the cells. Afterwards, lysed suspension was cast onto the electrode surface, deposited for 3 min and measured by DPV.

Inductively Coupled Plasma Mass Spectrometry (ICP-MS)

The determination of the total concentration of ruthenium in cells was done by ICP-MS Agilent 7900 (Agilent Technologies). Before the analysis, the cell pellets were mixed with 1 ml of 5% nitric acid. This mixture was placed in an ultrasonic bath for 3 min to lyse the cells and subsequently was diluted by MiliQ water by factor 10. A solution of Ni and Rh (10 ng/ml) was used as an internal standard (IS) to suppress matrix effect, and possible instrument drift during measurement. ICP-MS parameters were optimized for getting the highest signal-to-noise ratio while oxide ratio is lower than 1.5%. Isotopes ^{57}Fe, ^{60}Ni, ^{101}Ru, and ^{103}Rh were used for all measurements. Set of calibration standards (0-1-10-50-100 µg/l and 0-0.1-1-10-50 µg/l of Fe and Ru, respectively) was used for quantification. The obtained limit of detection was 0.4 and 0.01 µg/l of Fe and Ru.

Shake flask method

4 and **6** were dissolved to the 20mM concentration in DMSO. These stocks of **4** and **6**, respectively were added into water and 1-octanol to a final concentration of 1mM. The same volumes of water and octanol containing **4** or **6** were mixed and shaken for 5 min. Then the tubes were shortly spun and samples from aqueous and organic layer were subjected to UV/VIS spectrophotometry (NanoDrop 2000, ThermoFisher Scientific). Absolute amounts of **4** and **6** were calculated by constructing calibration curves (Figure S20). LogP was defined as the logarithm of the ratio of the concentrations of a solute between the two solvents.

Cytotoxicity testing

Cells were seeded in density 3000 cells per well in 96-well plate and incubated with selected compounds for 72 h. Then the cell viability was measured using colorimetric MTT assay as described previously.[13] Data from cytotoxicity assay were analyzed in GraphPadPrism software and expressed as IC_{50} values (compound concentrations that produce 50% of cell metabolic inhibition). All experiments were made independently in triplicates.

Cell cycle determination

2×10^5 cells were seeded in 6 well plates and afterwards treated with 10 μM **4** or **6** for 48h. The cells were washed twice with PBS and fixed in 70% ethanol overnight at 4 °C. The cells were then washed with PBS and stained with 1 ml of PI staining solution per sample (0,1% Triton X-100, 10 μg/ml propidium iodide, 100 μg/ml DNAse free RNAase A, all Sigma-Aldrich, St. Louis, USA) for 30 minutes at room temperature in the dark. After incubation, the fluorescence was measured at flow cytometer (FACS Verse, BD Biosciences, Franklin Lake, New Jersey, USA) and evaluated using BD FACSuite v 1.0.6. Total of 10,000 events per sample were recorded.

Annexin V cell death analysis

10^5 cells were seeded in 12 well plates and then treated with 10 μM **4** or **6** for 24h. Afterwards the cells were collected with acutase and washed twice with PBS. Cell pellets were then resuspended in 50 μl of staining solution prepared from 1× binding buffer (20× Annexin V Binding Buffer, MACS Miltenyi Biotec), 1 μl of FITC-Annexin V (Biolegends, San Diego, USA), and 0,5 μl of 1 mg/ml PI (Sigma-Aldrich, St-Louis, USA) and incubated for 20 minutes in the dark at room temperature. The fluorescence signal was detected at flow cytometer (FACS Verse, BD Biosciences, Franklin Lakes, New Jersey, USA). A total of 10,000 events were recorded for each sample. The percentage of apoptotic cells was quantified using FCS Express 4 software (BD Biosciences, Franklin Lakes, New Jersey, USA)

Wound healing assay

Confluent cells grown in 12 well plates were scraped with a sterile micropipette tip and afterwards incubated in serum-free DMEM with given concentrations of aforementioned compounds. Time-lapse acquisition of the wound closure was detected on Nicon Eclipse Ti-E system at 10× magnification. The pictures were captured at three randomly chosen fields within the wound region every 4 hours for 24 h. The migration rate was assessed using TScratch software[27] by quantification of the cell-free area 24 h post-scratching.

Statistical analysis

One-way ANOVA (analysis of variance) with post-hoc Tukey HSD calculator was used to determine statistically significant differences between the groups generated from at least three

independent experiments unless otherwise stated. It was performed using the free online web tool available at https://astatsa.com/OneWay_Anova_with_TukeyHSD/. Tests with $P<0.05$ were considered as significant. The error bars represent the standard deviation of corresponding data sets.

Acknowledgement

This work was supported by Czech Science Foundation (project 17-05838S), Ministry of Health of the Czech Republic (project MMCI 00209805), and Ministry of Education, Youth and Science (project NPS I-LO1413). G.D. thanks to Central European Exchange Programme for University Students (project CIII-RO-0010-14). J.P. thanks Dr. L. Petrusova for melting points determinations.

References

[1] a) G. Jaouen, A. Vessieres, S. Top, *Chem. Soc. Rev.* **2015**, *44*, 8802-8817; b) K. Kowalski, *Coord. Chem. Rev.* **2016**, *317*, 132-156; c) A. Singh, I. Lumb, V. Mehra, V. Kumar, *Dalton Trans.* **2019**, *48*, 2840-2860.

[2] a) E. Alessio, *Eur. J. Inorg. Chem.* **2017**, 1549-1560; b) B. S. Murray, M. V. Babak, C. G. Hartinger, P. J. Dyson, *Coord. Chem. Rev.* **2016**, *306*, 86-114.

[3] S. Thota, D. A. Rodrigues, D. C. Crans, E. J. Barreiro, *J. Med. Chem.* **2018**, *61*, 5805-5821.

[4] a) G. Von Poelhsitz, A. L. Bogado, M. P. de Araujo, H. S. Selistre-de-Araujo, J. Ellena, E. E. Castellano, A. A. Batista, *Polyhedron* **2007**, *26*, 4707-4712; b) C. H. Mu, S. W. Chang, K. E. Prosser, A. W. Y. Leung, S. Santacruz, T. Jang, J. R. Thompson, D. T. T. Yapp, J. J. Warren, M. B. Bally, T. V. Beischlag, C. J. Walsby, *Inorg. Chem.* **2016**, *55*, 177-190.

[5] a) M. Auzias, B. Therrien, G. Suss-Fink, P. Stepnicka, W. H. Ang, P. J. Dyson, *Inorg. Chem.* **2008**, *47*, 578-583; b) M. Auzias, J. Gueniat, B. Therrien, G. Suss-Fink, A. K. Renfrew, P. J. Dyson, *J. Organomet. Chem.* **2009**, *694*, 855-861; c) C. H. Mu, K. E. Prosser, S. Harrypersad, G. A. MacNeil, R. Panchmatia, J. R. Thompson, S. Sinha, J. J. Warren, C. J. Walsby, *Inorg. Chem.* **2018**, *57*, 15247-15261.

[6] J. Tauchman, G. Suss-Fink, P. Stepnicka, O. Zava, P. J. Dyson, *J. Organomet. Chem.* **2013**, *723*, 233-238.

[7] P. Govender, H. Lemmerhirt, A. T. Hutton, B. Therrien, P. J. Bednarski, G. S. Smith, *Organometallics* **2014**, *33*, 5535-5545.

[8] K. Kowalski, M. Linseis, R. F. Winter, M. Zabel, S. Záliš, H. Kelm, H.-J. Krüger, B. Sarkar, W. Kaim, *Organometallics* **2009**, *28*, 4196-4209.

[9] I. Ott, K. Kowalski, R. Gust, J. Maurer, P. Mücke, R. F. Winter, *Bioorg. Med. Chem. Lett.* **2010**, *20*, 866-869.

[10] M. M. Milutinovic, P. P. Canovic, D. Stevanovic, R. Masnikosa, M. Vranes, A. Tot, M. M. Zaric, B. S. Markovic, M. M. Marjanovic, L. Vucicevic, M. Savic, V. Jakovljevic, V. Trajkovic, V. Volarevic, T. Kanjevac, A. R. Simovic, *Organometallics* **2018**, *37*, 4250-4266.

[11] a) J. Schulz, F. Uhlik, J. M. Speck, I. Cisarova, H. Lang, P. Stepnicka, *Organometallics* **2014**, *33*, 5020-5032; b) E. A. Ziemann, S. Baljak, S. Steffens, T. Stein, N. Steerteghem, I. Asselberghs, K. Clays, J. Heck, *Organometallics* **2015**, *34*, 1692-1700.

[12] S. Bhattacharyya, *J. Org. Chem.* **1998**, *63*, 7101-7102.

[13] T. Hodik, M. Lamac, L. Cervenkova Stastna, P. Curinova, J. Karban, H. Skoupilova, R. Hrstka, I. Cisarova, R. Gyepes, J. Pinkas, *J. Organomet. Chem.* **2017**, *846*, 141-151.

[14] R. M. Fairchild, K. T. Holman, *Organometallics* **2007**, *26*, 3049-3053.

[15] R. A. Zelonka, M. C. Baird, *J. Organomet. Chem.* **1972**, *44*, 383-&.

[16] a) A. R. Kudinov, M. I. Rybinskaya, Y. T. Struchkov, A. I. Yanovskii, P. V. Petrovskii, *J. Organomet. Chem.* **1987**, *336*, 187-197; b) B. T. Loughrey, B. V. Cunning, P. C. Healy, C. L. Brown, P. G. Parsons, M. L. Williams, *Chem.-Asian J.* **2012**, *7*, 112-121.

[17] a) O. V. Gusev, M. A. Ievlev, M. G. Peterleitner, S. M. Peregudova, L. I. Denisovich, P. V. Petrovskii, N. A. Ustynyuk, *J. Organomet. Chem.* **1997**, *534*, 57-66; b) S. K. Mohapatra, A. Romanov, T. V. Timofeeva, S. R. Marder, S. Barlow, *J. Organomet. Chem.* **2014**, *751*, 314-320.

[18] a) M. Bartosik, L. Koubkova, J. Karban, L. Cervenkova Stastna, T. Hodik, M. Lamac, J. Pinkas, R. Hrstka, *Analyst* **2015**, *140*, 5864-5867; b) H. Skoupilova, M. Bartosik, L. Sommerova, J. Pinkas, T. Vaculovic, V. Kanicky, J. Karban, R. Hrstka, *Eur. J. Pharmacol.* **2020**, *867*, 172825.

[19] C. A. Lipinski, F. Lombardo, B. W. Dominy, P. J. Feeney, *Adv. Drug Delivery Rev.* **2001**, *46*, 3-26.

[20] H. Kostrhunova, E. Petruzzella, D. Gibson, J. Kasparkova, V. Brabec, *Chem.-Eur. J.* **2019**, *25*, 5235-5245.

[21] B. T. Loughrey, P. C. Healy, P. G. Parsons, M. L. Williams, *Inorg. Chem.* **2008**, *47*, 8589-8591.

[22] J. M. Wagner, L. M. Karnitz, *Mol. Pharmacol.* **2009**, *76*, 208-214.

[23] R. G. Kenny, C. J. Marmion, *Chem. Rev.* **2019**, *119*, 1058-1137.

[24] P. J. Fagan, M. D. Ward, J. C. Calabrese, *J. Am. Chem. Soc.* **1989**, *111*, 1698-1719.

[25] G. M. Sheldrick, *Acta Crystallogr. Sect. C-Struct. Chem.* **2015**, *C71*, 3-8.

[26] A. L. Spek, *Acta Crystallogr. Sect. D-Biol. Crystallogr.* **2009**, *D65*, 148-155.

[27] T. Geback, M. M. Schulz, P. Koumoutsakos, M. Detmar, *Biotechniques* **2009**, *46*, 265-274.

10.1002/cplu.202000022

Graphical abstract

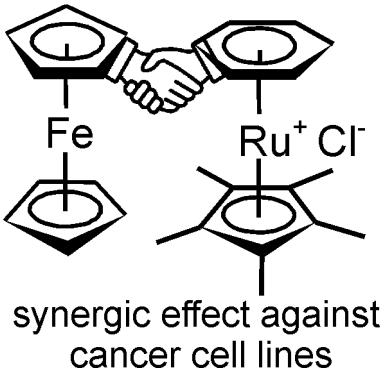

Together we are stronger: Dinuclear and trinuclear ferrocene-cationic ruthenium arene conjugates show higher potency against selected cancer cell lines (A2780, SK-OV-3, MDA-MB-231) than the isolated components. The ferrocene core involved in both conjugates allowed simple determination of conjugates cellular uptake by differential pulse voltammetry (DPV). The dinuclear conjugate displays approximately two times higher intracellular accumulation in comparison to the trinuclear one, which roughly corresponds to its higher cytotoxicity.

keywords: antitumor agents; electrochemistry; ferrocene; metallocene; ruthenium